HEAVY ION FUSION REACTIONS AROUND THE COULOMB BARRIER

A Dissertation submitted

in the partial fulfilment of the requirement for the degree of

MASTERS OF SCIENCE

In

PHYSICS

Submitted by

Garima
Roll no. 301704007

Under the Guidance of

Dr. Sunil Devi
Assistant Professor, SPMS

School of Physics and Material Science (SPMS)

Thapar Institute of Engineering & Technology

Patiala, Punjab-147004

July-2019

A grateful heart is a beginning of greatness

I dedicate this thesis to my parents VINOD KUMAR and NEELAM SHARMA. I hope this achievement fulfills your dream to give me the best education.

Certificate

This is to certify that the work represented in the thesis entitled **HEAVY ION FUSION REACTIONS AROUND THE COULOMB BARRIER,** submitted towards the partial fulfilment of **Master of Science (Physics)** degree submitted in the **School of Physics and Materials Science (SPMS)** of **Thapar Institute of Engineering and Technology (TIET),** is an authentic record of work carried out by me under the guidance of Dr. Sunil Devi, **SPMS, TIET**. The matter embodied in this thesis has not been submitted in part or full to any other university or institute for the award of any degree.

Garima
(Garima)

Date 10th July 2019

This is to certify that above declaration made by the student concerned is correct to the best of my knowledge.

Sunil
Dr. Sunil Devi

(Asst. Professor)

SPMS, TIET, Patiala

Acknowledgements

I would like to thank all the people who supported me through my M.Sc. I would like to express my deepest gratitude to **Dr. Sunil Devi** for her lectures on nuclear physics and helping me with deciding the topic for my thesis work. I am thankful to her for all the discussions regarding the topic. Her suggestions at every step of the thesis work were always helpful to me. It was a very good learning experience to work under her supervision.

I would also like to thank Mr. Shoaib Noor, Ph.D. scholar, TIET, who helped me with the basics of the fusion and work related to the subject.

I am blessed for the support of my family and friends. I would like to thank my best friend and my well-wisher Harman for motivating me throughout my M.Sc. and my friends Trisha Walia, Arshjot Kaur, Bhaktima for their support and with whom I created unforgettable memories.

Garima

Date: 10th July 2019

Abstract

The LISE++ package is used to simulate heavy ion fusion reactions. The simulations are done using the code PACE4 at energies around the Coulomb barrier. Formation of compound nucleus (CN) and evaporation residues in the interactions of ^{28}Si with ^{76}Ge and ^{30}Si with ^{74}Ge is studied as a function of incident beam energy. These two systems are chosen because they populate the same compound nucleus ^{104}Pd. Simulations are performed for estimating complete fusion cross sections from 20% below to 20% above the Coulomb barrier. The effect of varying the beam energy was analysed by plotting partial cross sections as a function of total angular momentum, the change in angular distribution of evaporation residues with beam energy and the angular distribution of protons, neutrons and alpha particles.

Table of contents

List of Figures

List of Tables

Chapter 1

INTRODUCTION

1.1 INTRODUCTION

The branch of physics that studies atomic nuclei and their constituents along with their interactions can be referred as *Nuclear physics*. A nuclear reaction is a process in which nuclei/nucleons interact to produce new nuclear states, particles, x-rays and gamma rays. There are many applications of nuclear physics which includes nuclear power, nuclear reactors, nuclear imaging of diseases, diagnosing and curing medical conditions, radio-immunotherapy etc. Nuclear reactions power the energy production of stars. In nuclear physics, we study about nuclear decays, nuclear structure and nuclear reactions [1]. In this chapter, different type of nuclear reactions, heavy ion fusion reactions, tunneling through the Coulomb barrier etc. are discussed.

Representation of a Nuclear Reaction:

If $\mathbf{X_1}$ and $\mathbf{X_2}$ are the initial nuclei and $\mathbf{Y_1}$ and $\mathbf{Y_2}$ are the product nuclei, the reaction can be represented as follows:

$$X_1 + X_2 \rightarrow Y_1 + Y_2$$

Or

$$X_1(X_2, Y1)\ Y2$$

1.2 CLASSIFICATION OF NUCLEAR REACTIONS

On basis of interaction time nuclear reactions can be classified as direct reactions and compound nuclear reactions.

- *Direct reactions:* These are those reactions which occur for a very short time and only allow interaction of single/few nucleon. In these reactions, surface of target nucleus interacts with incident particles. The interaction time for direct reaction is of order of 10^{-22} second which shows that they occur very rapidly. In direct reactions, products are forward focused thus are not distributed isotropically. The angular distributions of ongoing particles have sharp peak. The different types of direct reactions are :

a) *Elastic scattering*: In these reactions, the initial and final kinetic energy of projectile is same. After the interaction, both projectile and target nuclei are in ground state. The incident particle is deflected due to the Coulomb field of the target nucleus.

b) *Inelastic scattering*: It is possible that projectile particle will gives off some of energy to target nucleus which leads to excitation of target nucleus and that much energy is absorbed from kinetic energy of projectile. The projectile nucleus can be inelastically excited to one of its higher states. The kinetic energy of the outgoing incident particle will be less. Inelastic scattering could be either due to Coulomb or nuclear excitation.

c) *Transfer reactions*: In these reactions, there is exchange of one or more nucleons between projectile and target nucleus. If nucleons are transferred from projectile to target, it is called stripping reaction. Whereas, if nucleons are transferred from target to projectile, it is called as pick-up reaction. Transfer reactions can be accompanied by inelastic scattering.

- *Compound nucleus reactions:* These reactions involve a large number of interactions between nucleons of projectile and target. In these reactions, volume of the target nucleus interacts with the incident particle. The interaction time for compound nuclear reaction is of order of 10^{-18}- 10^{-16} second, which is longer compared to direct reaction and observed life-time of compound nucleus will be 10^{-14} second. Reaction Products are distributed isotropically in compound nucleus reactions. In these

reactions, leaving particles have less sharply peaked angular distribution as compared to direct reaction.

Direct reactions and compound nucleus reactions are very common processes with heavy ions (A≥4).

1.3 HEAVY ION FUSION REACTIONS

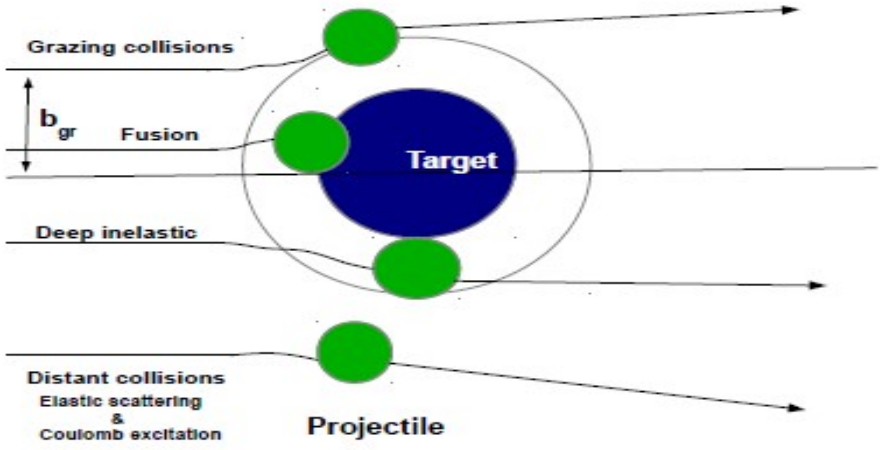

Fig. 1.1 Different processes observed in heavy ion collisions as a function of impact parameter.

A *heavy ion* is generally defined as nucleus with mass number greater than or equal to four i.e. A ≥ 4. For heavy ions fusion reactions to occur, the incident particle needs to be accelerated as there is Coulomb repulsion between the interacting nuclei. There are accelerators which can produce heavy ion beam of energy in the range from few MeV/nucleon to GeV/nucleon. The different processes which can take place in heavy ion reactions are as shown in Fig.1.1.

Impact parameter can be defined as the perpendicular distance between centre of mass of the interacting nuclei. When impact parameter is large, Coulomb effects will dominate and Coulomb excitation may occur. When overlapping starts in the nuclear wave functions of the target and projectile, then nuclear reactions occur. At small impact parameter, compound nucleus is formed when nuclei overlap completely, which represents complete fusion of those nuclei and an intermediate state is formed.

However, incident ion should be quite energetic to overcome the repulsive Coulomb barrier and thus with some considerable excitation energy compound nucleus is formed [3].

Fig. 1.2 shows three steps which are involved in fusion process:

I. *Approaching and capture process*: Target nucleus will be approached by projectile nucleus and it will penetrate fusion barrier, and both the nuclei will contact each other.

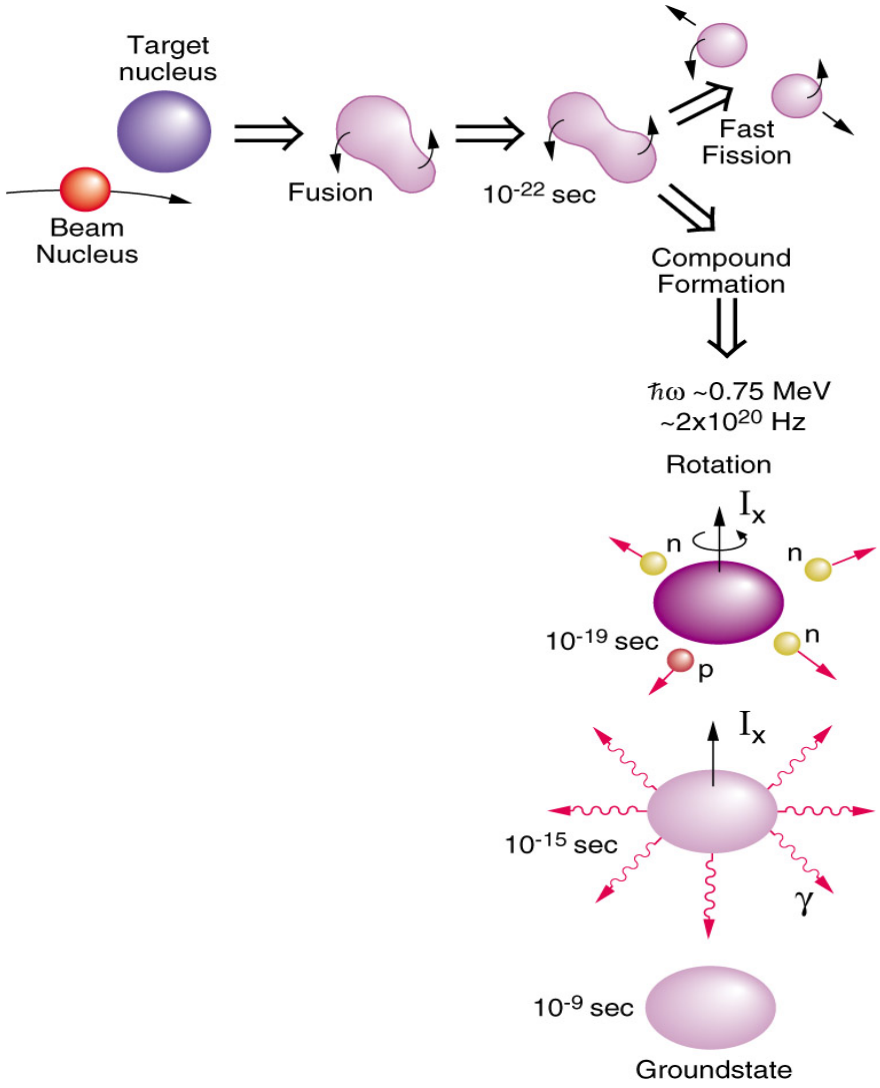

Fig. 1.2 Fusion evaporation reactions.

II. *Formation of compound nucleus*: After contact, the composite system will evolve into the compound nucleus (CN) formation. Because of strong Coulomb repulsion force, the creation of compound nucleus competes with re-separation. With increase in the charge product of the target nucleus and projectile nucleus, the re-separation becomes dominant.

III. *Evaporation process:* The compound nucleus which is initially excited will now de-excite and will form evaporation residues (ERs). There will be emission of neutron, proton, alpha particles, and γ –rays. If the mass of compound system is large, fission is dominant.

1.4 FUSION REACTIONS AROUND THE COULOMB BARRIER

The fusion of atomic nuclei is most impressive process in nature. The total potential is sum of the long range Coulomb repulsive force, centrifugal term and short range nuclear attractive force. The total interaction potential can be given as

$$V = V_C(r) + V_N(r) + \frac{\hbar^2 l(l+1)}{2\mu r^2}$$

where V is total interaction potential, r is distance between projectile and target, l is angular momentum quantum number and μ is the reduced mass of the system.

$V_N(r)$ is attractive nuclear potential, taken to be of Woods-Saxon form [7].

$$V_N(r) = \frac{-V_0}{1+exp\{\frac{r-R_0}{a}\}}$$

where V_0 is potential well depth, a represents surface thickness and $R_0 = r_0 A^{1/3}$ is nuclear radius (A represents mass number).

$V_C(r)$ is the Coulomb potential given by,

$$V_C(r) = \frac{e^2}{4\pi\epsilon_\circ}\frac{Z_a Z_b}{r}$$

where Z_a and Z_b are charges on projectile and target particles respectively.

The fusion cross section is given by

$$\sigma_F = \frac{\pi}{k^2}\sum_{l=0}^{\bowtie}(2l+1)T_l(E) = \sum_{l=0}^{\bowtie}\sigma_F(l,E)$$

where, $\sigma_F(l,E)$ is partial fusion cross section.

$T_l(E)$ is transmission coefficient.

If r is very large it means that projectile is going to interact with nucleus through the Coulomb interaction. For very small energy of this projectile nucleus, projectile will not able to tunnel through the barrier and it is then just scattered elastically and of course it is not nuclear reaction in this case instead, it is *coulomb interaction*. Now if we increase energy and it is able to penetrate into nuclear region, then different types of nuclear reactions will occur [3].

Chapter 2

LITERATURE REVIEW

2.1 INTRODUCTION

In this chapter, research interests and various measurements performed around the Coulomb barrier are presented. A review on LISE ++ software is also presented in this chapter.

2.2 LITERATURE SURVEY

Many studies are available in the literature on the heavy ion fusion reactions for different systems. **C.Y.Wong** [8] gives expressions experimentally, which allows the interaction barrier to be determined. Their analysis of experimental data of heavy ion on ^{238}U which will give the effective radius parameter details that it will decreases as projectile charges increases. Firstly, it is discussed that the measurement of height of barrier will provides information about the fusion process. It is important for the production of super heavy nuclei by heavy ion reactions. The barrier can be obtained by analyzing the reaction cross section or elastic scattering with an optical model. There is another way to predict about Coulomb barrier through expressions obtained in ingoing wave strong absorption model. Here in this physical review author considers two spherical nuclei. No dynamic distortion is taken into account. Hill-Wheeler formula will give probability for absorption of l^{th} partial wave and total reaction cross section is obtained. In further steps effective potential for the reaction is obtained.

A.Gavron [9] attempts calculations using simple level density parametrization, to examine experimental data for different heavy ion reactions. They tell that the occurrence of heavy ion accelerators will make nuclei's study easier when there is high angular momentum and excitation energy. Study of evaporation residues cross section and gamma ray multiplicity shows that there will be a linear correlation between maximum angular momentum of evaporation-residues, l_{max} and average gamma ray multiplicity, M_{γ}.

There were considered many reactions like Ar + ^{109}Ag, Ar + ^{118}Sn, Ar + ^{124}Sn, Ne + ^{150}Nd and Ar + Te. They supposed decay properties of the excited nuclei can be given by the statistical model calculations. After analyzing all reactions, they find difference in results of statistical model calculations and experimental calculations. The purpose of their study in terms of evaporation calculations was to study the quantity to which available data can be interpreted using Fermi gas level parameterization. The information which was obtained in these statistical calculations are - relative cross section for *xn* and *xnα* reactions, average angular momentum which will leads to exact *xn* channels (which was given by multiplicity measurements) and critical angular momentum which will limits the existence of evaporation residues.

Tarasov et. al. [10] developed *LisFus,* a fresh fusion-evaporation model for doing quick estimation of fusion residue cross-sections. It was a further development of *LISE* program. This type of model can be used to determine very little cross-sections rapidly because of comparison with other programs by means of Monte Carlo simulation. Fast calculation is essential for the estimation of fusion residue yields. Using LisFus model, LISE program has the possibility to analyse the fusion residue's transmission from a fragment separator. Also in this paper, Tarasov et. al. gave a possible use of fusion residues cross-section which can be calculated by the program *PACE*. Comparison of *PACE* and *LisFus* model was presented in this paper. In LISE framework, PACE4 program has numerous new characteristics like having a user-friendly interface in which user can enter information, can plot calculated cross-sections possibly using LISE program whereas LisFus which is new fusion evaporation model is based upon the Bass fusion cross-section algorithm.

Kalkal et. al. [11] measured the fusion excitation functions in interactions of ^{28}Si with ^{90,94}Zr targets around the Coulomb barrier. The experimental fusion cross sections are compared with theoretical predictions using coupled channel calculations. The authors concluded that transfer reactions having positive Q-values strongly influence the fusion cross sections around the Coulomb barrier. Therefore, a strong isotopic dependence of fusion cross sections is observed.

Jia et. al. [13] measured fusion excitation function with high accuracy for $^{16}O + ^{76}Ge$ and $^{18}O + ^{74}Ge$ systems. The measurements were performed at energies near the Coulomb barrier and below the Coulomb barrier. The channel coupling effects of positive Q-value neutron transfer channels are main focus of this study. At sub-barrier energies, no fusion cross section enhancement was observed for $^{18}O + ^{74}Ge$ in comparison to $^{16}O + ^{76}Ge$. Fusion cross sections for both the systems are similar even though $^{18}O + ^{74}Ge$ has positive Q-value for two neutron transfer channel.

Aljuwair et. al. [14] measured the fusion excitation functions for $^{40}Ca + ^{40,44,48}Ca$. Strong isotopic dependence was observed suggesting the importance of channel coupling of transfer reactions in fusion reactions.

Zhang et. al.[15] also measured fusion excitation functions with good accuracy at near and below the Coulomb barrier for the first time for system $^{32}S + ^{90}Zr$ and $^{32}S + ^{96}Zr$. The sub-barrier fusion cross sections for $^{32}S + ^{96}Zr$ were found to be much enhanced as compared to $^{32}S+^{90}Zr$. The data analysis was carried out using channel coupling approach and channel coupling effect of neutron transfer reactions was implied. Fusion and quasi-elastic barrier distribution for these systems were found to be consistent.

Chapter 3

SOFTWARE AND METHODOLOGY

3.1 INTRODUCTION

This Chapter describes the program which is used to analyze the heavy ion fusion reaction around the Coulomb barrier and theoretical calculations.

3.2 PROGRAM LISE++

The program LISE was developed to analyze various things like transmission and yields of fragments formed and obtained in a fragment separator. The *LISE* ++ has following format:

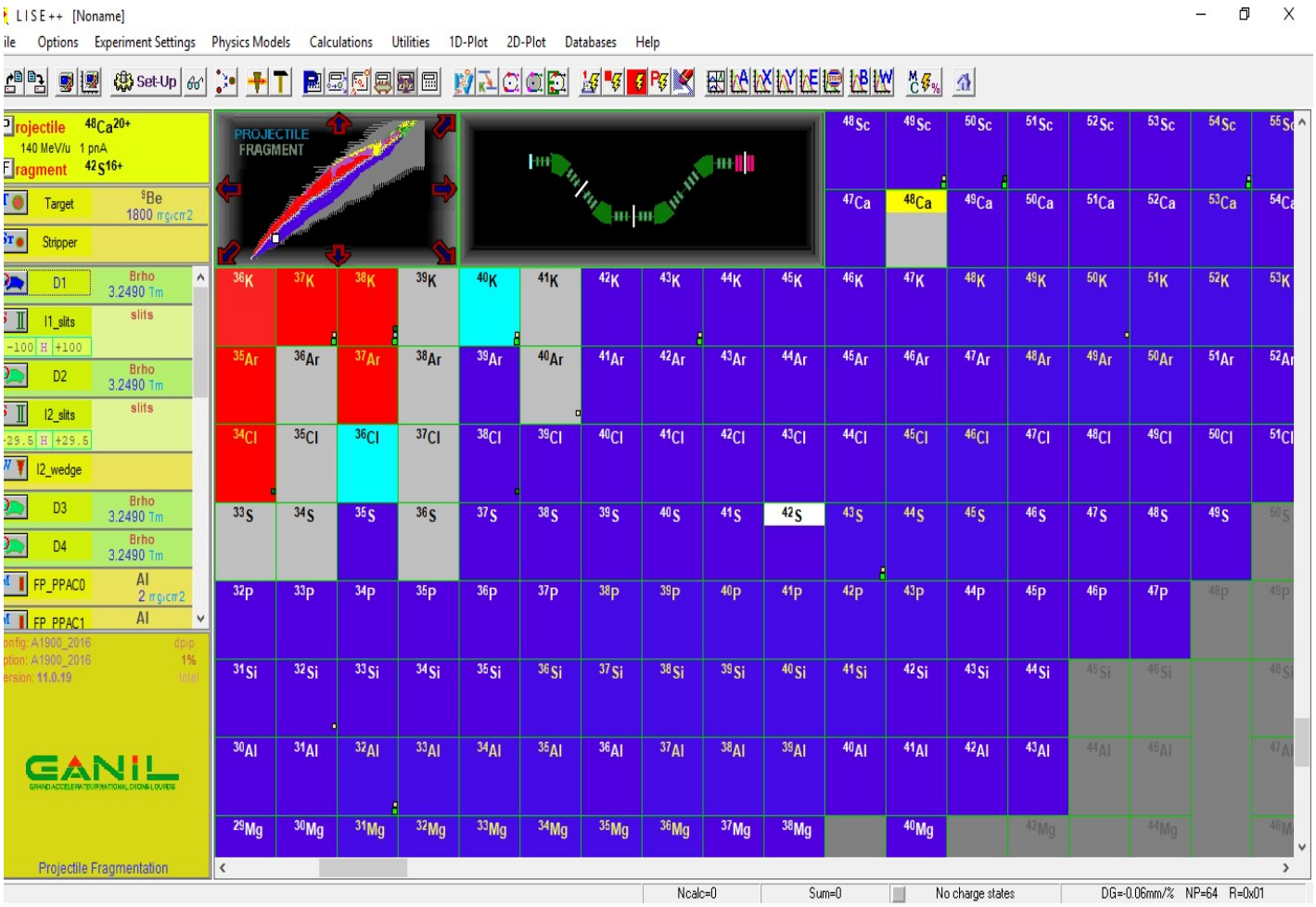

Fig. 3.1 Format of LISE ++ software.

LISE will allow to fully simulate the formation of radioactive beams, from the parameters of the reaction method to the detection of the nuclei which was selected by the fragment separator. This program is extremely user friendly, which was designed as tuning tool during experiments where its results can be rapidly compared to on-line data. Built-in Energy loss, cross-section distribution plots, angular distribution, charge and cross-section distribution plots and dE-E, Z-A/Q and dE-X two-dimensional plots allows simulating the experimental observables.

3.3 CODE PACE4

In the LISE framework, fusion reactions are simulated using PACE code which is based on paper by A. Gavron [9] and is advanced edition of JULIAN- the Hillman-Eyal evaporation code. The program PACE4 has input file of the following format:

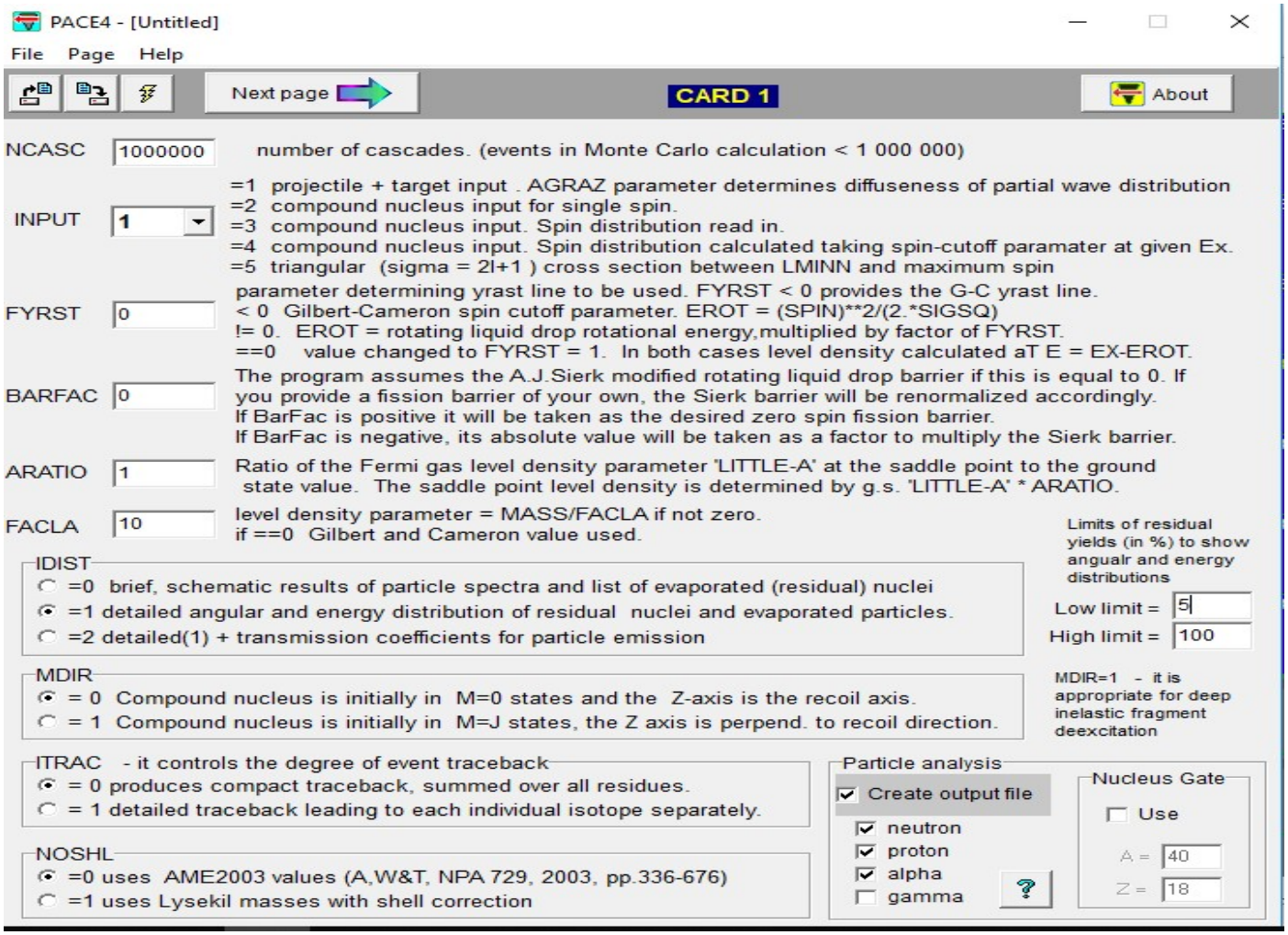

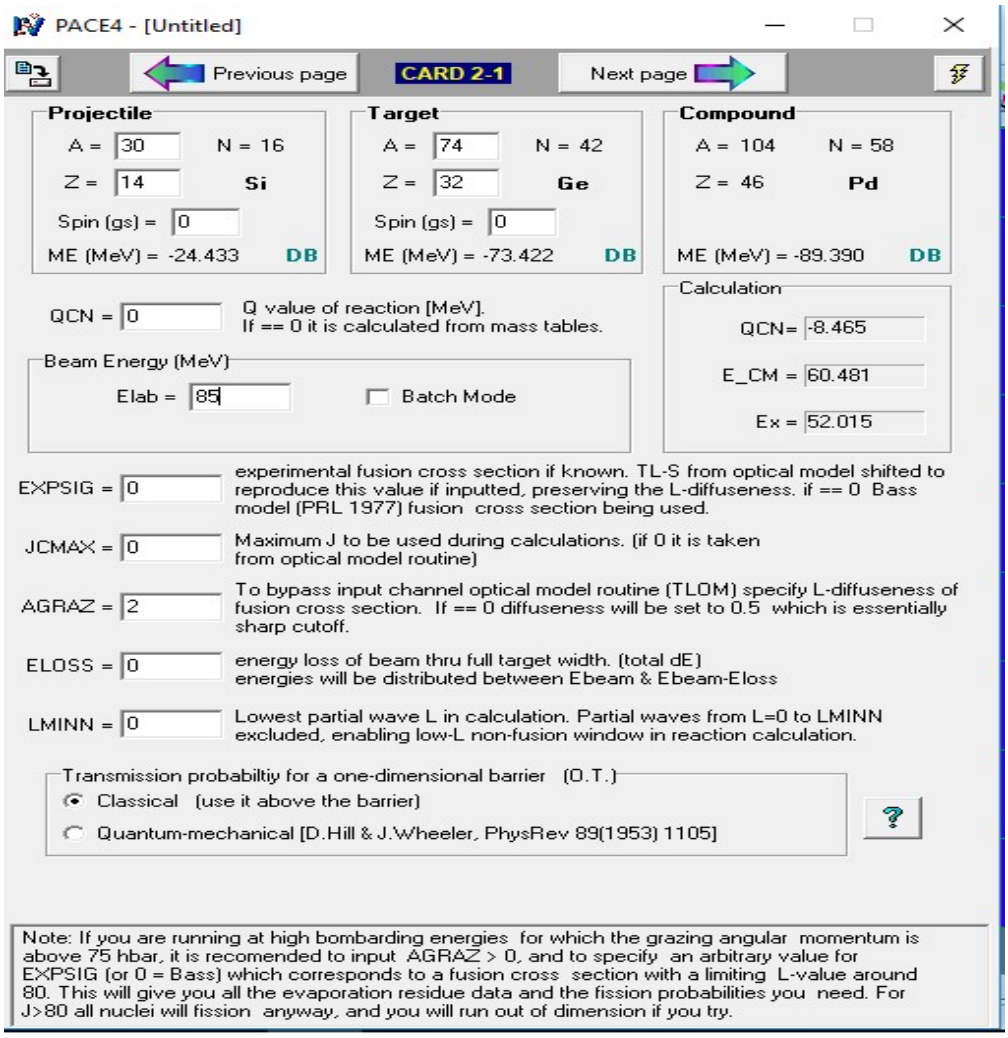

Fig. 3.2 Format Of PACE4 input file.

The PACE which stands for *Projection Angular-momentum Coupled Evaporation* is statistical model evaporation code which is used to simulate the main evaporation channels in fusion reactions at different laboratory beam energies. It uses Monte-Carlo simulation for de-excitation of compound nucleus. The major advantage of Monte-Carlo simulation is that it will provide correlation between various quantities. The code calculates probabilities and decay widths for all the nuclei which are present in the decay chain. It happens till the residual nuclei will no longer decay. Energy spectra and angular distribution of emitted particles can be obtained from this code. The code also gives the evaporation residue cross section as well as fission cross-section. It is possible to calculate up to 1000000 cascades at excitation energy of 2000 MeV.

In Fig. 3.2, NCASC stands for number of cascades i.e. number of events in Monte- Carlo calculations upto 1000000. INPUT will have values from 1 to 5 according to conditions given by systems. INPUT will have value 1 for projectile and target input. Several different parameters are considered for determining INPUT value. Some default values are FACLA is taken as equal to 8 and AGRAZ parameter should be taken equal to 2 for this version of PACE4 and IDIST should be less than 0 for particle analysis. Limit of residual yield in % is set to show energy and angular distributions. In Fig. 3.2, also A and Z of projectile and target stands for mass number and atomic number respectively. Also, A and Z for compound nucleus will be obtained automatically. Beam energy is in MeV, Elab stands for energy value for which simulation is to be carried out. Transmission probability for a one-dimensional barrier is calculated using classical model at above-barrier energies and quantum mechanically at sub-barrier energies. The excitation energy in Fig. 3.4 shows current step in batch mode.

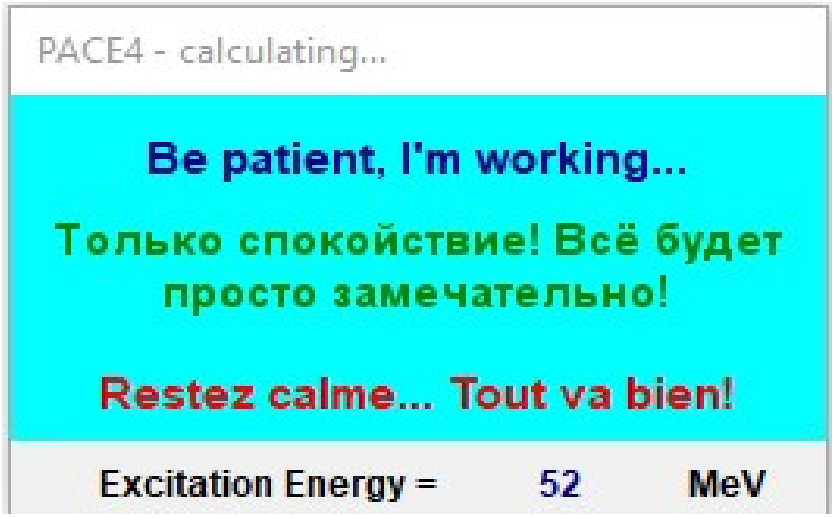

Fig. 3.3 Example of calculations in PACE4

3.4 WORK PLAN

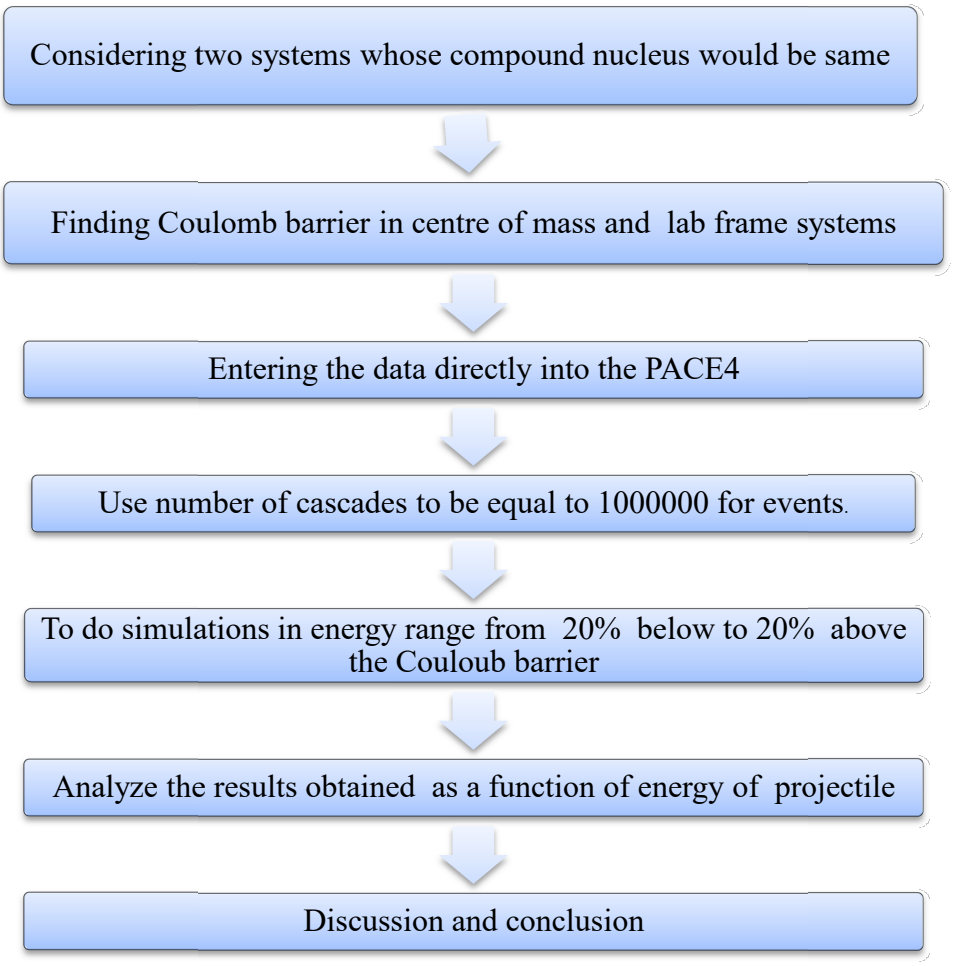

Fig. 3.4 Flowchart of Work-plan.

Chapter 4

RESULTS AND DISCUSSIONS

4.1 Introduction

As discussed in previous chapters, after entering all the required data, output is obtained at different energies. Three energies are considered –below the Coulomb barrier, above the Coulomb barrier and near the Coulomb barrier. The following section discusses all the simulation work carried out in present thesis.

4.2 Systems Details

Reactions in interactions of ^{28}Si with ^{76}Ge and ^{30}Si with ^{74}Ge are considered because they will give us same compound nucleus after fusion i.e. ^{104}Pd.

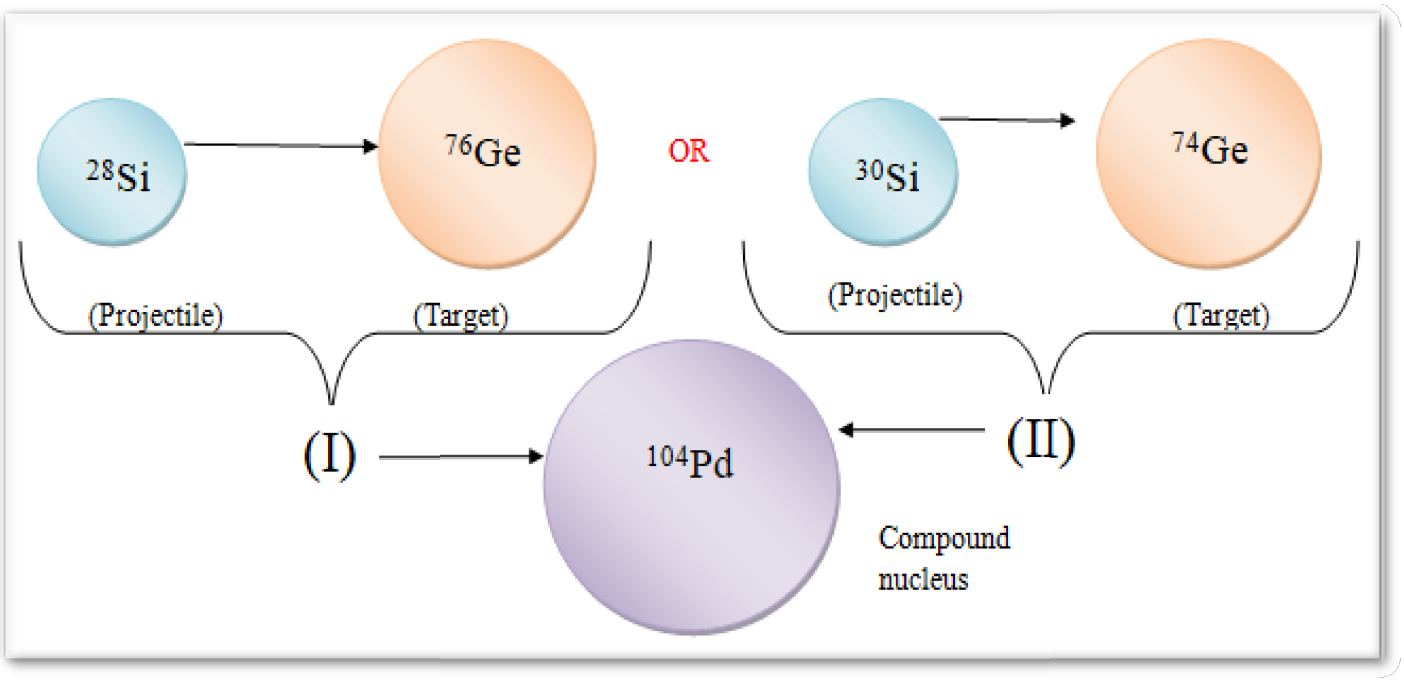

Fig. 4.1 Illustration of considered reactions of of ^{28}Si with ^{76}Ge and ^{30}Si with ^{74}Ge to form same compound nucleus.

As we know, the Coulomb barrier is given by (for centre of mass frame),

$$(V_C)_{\text{centre of frame}} = \frac{e^2}{4\pi\epsilon_\circ}\frac{Z_a Z_b}{R_a+R_b}$$

where $R_a = R_o A_a^{1/3}$ and $R_b = R_o A_b^{1/3}$

Now we have to calculate V_c for lab frame as all calculations should be done in lab frame itself. So,

$$(V_c)_{\text{lab frame}} = \frac{A_{CN}}{A_T}(V_c)_{centreofframe}$$

So, the calculated Coulomb barriers in interactions of ^{28}Si with ^{76}Ge and ^{30}Si with ^{74}Ge are given in table 4.2.

Table 4.2 Value of the Coulomb barrier for centre of mass frame and in lab frame in interactions of ^{28}Si with ^{76}Ge and ^{30}Si with ^{74}Ge.

System	(V_B) in CM	(V_B) in lab frame
^{28}Si + ^{76}Ge	63.37 MeV	86.716 MeV
^{30}Si + ^{74}Ge	63.07 MeV	88.582 MeV

Reaction information is provided into PACE4. Number of cascades to maximum value i.e. 1000000 for events of Monte Carlo simulations. As we are considering projectile and target input, so our input will be 1. After all data inputs, PACE4 will gives evaporation residues. We will use beam energy below, above and near the Coulomb barrier. Also for transmission probability of one dimensional barrier is taken to be classical if we are using beam energy above the Coulomb barrier and quantum mechanical if we are using beam energy below the Coulomb barrier.

4.3 J VERSUS SIG (J)

The Fig. 4.2 shows angular momentum, J versus partial cross-section, SIG (J) plot for interactions of ^{28}Si with ^{76}Ge at energies below, near and above Coulomb barriers. As the beam energy increases, one can populate the high angular momentum states in compound nucleus. Hence, the graph goes to higher J as the beam energy is increased.

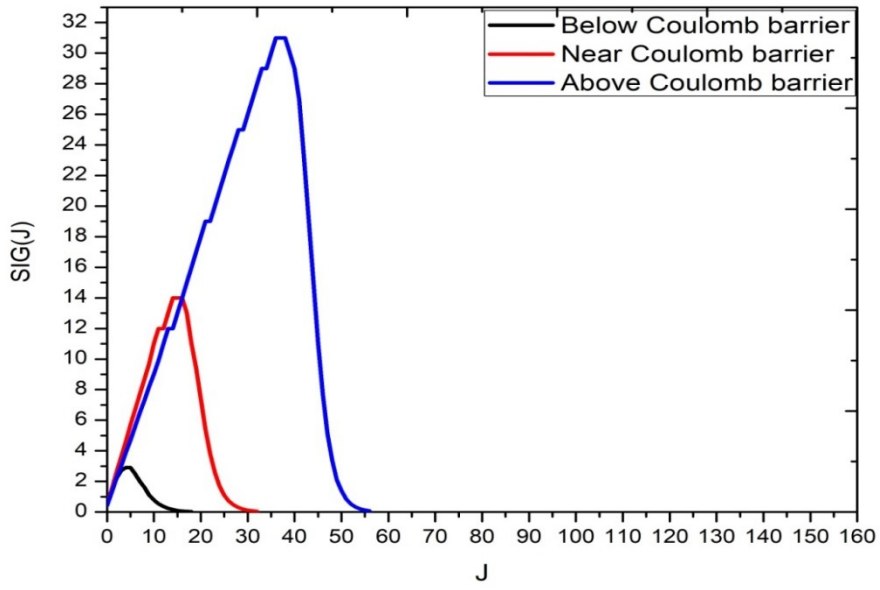

Fig. 4.2 J versus SIG (J) for $^{28}Si + ^{76}Ge$.

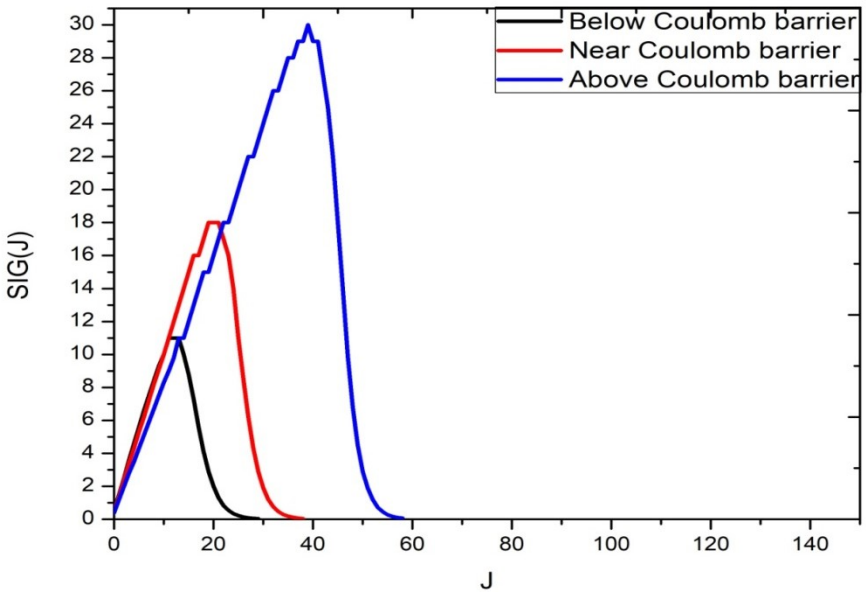

Fig. 4.3 J versus SIG (J) for $^{30}Si + ^{74}Ge$.

In Fig. 4.3 also angular momentum, J versus partial cross-section, SIG (J) is plotted. The plot is for interaction of ^{30}Si with ^{74}Ge at energies below, near and above Coulomb barrier. The observations are same as Fig. 4.2 that for above the Coulomb barrier, partial cross section can be populated up to high angular momentum states.

4.4 EVAPORATION RESIDUES AT DIFFERENT BEAM ENERGIES

Here Z is atomic number, N is neutron number, A is mass number for evaporation residues. The term Percentage yield (%) is defined as ratio of yield of that particular channel to total yield multiplied by 100. The cross section (SIG) is defined as the reaction probabilities. The cross section is expressed in units of area, its unit is barn (1 barn = $10^{-24}cm^2$ = $10^{-28}m^2$). Channel can be defined as the well defined quantum state in each reaction branch of the participants. The probability of a nuclear reaction to occur through a exit channel will depend upon the energy of incident particles and can be measured using the cross section of that channel.

For $^{28}Si + ^{76}Ge$:

(i) Below the Coulomb barrier

Table 4.2 Evaporation residues along with their Z, N, A, % yields, cross-section at energy below the Coulomb barrier for $^{28}Si + ^{76}Ge$.

Z	N	A	Evaporation Residue	Events	%	x-section	Channel
46	52	102	Pd	96772	9.68%	8.69E-07	2n
46	55	101	Pd	646781	64.7%	5.81E-06	3n
45	56	101	Rh	105011	10.5%	9.43E-07	1p2n
44	54	98	Ru	74492	7.45%	6.69E-07	2p4n

(ii) Near the Coulomb barrier

Table 4.3 Evaporation residues along with their Z, N, A, % yields, cross-section at an energy near the Coulomb barrier $^{28}Si + {}^{76}Ge$.

Z	N	A	Evaporation Residue	Events	%	x-section	Channel
46	55	101	Pd	45384	4.54%	8.99	3n
46	54	100	Pd	54336	54.3%	108	4n
45	55	100	Rh	220893	22.1%	43.8	1p3n
44	53	97	Ru	108103	10.8%	21.4	2p5n

(iii) Above the Coulomb barrier

Table 4.3 Evaporation residues along with their Z, N, A, % yields, cross-section at an energy above the Coulomb barrier $^{28}Si + {}^{76}Ge$.

Z	N	A	Evaporation Residue	Events	%	x-section	Channel
46	54	100	Pd	86936	8.69%	65.1	4n
45	55	100	Rh	50562	5.06%	37.9	1p3n
46	53	99	Pd	269208	26.9%	202	5n
45	54	99	Rh	269300	26.7%	202	1p4n
44	53	97	Ru	50214	5.02%	37.6	2p5n
44	52	96	Ru	158163	15.8%	119	2p6n

From above tables, one can conclude following about evaporation residues which are obtained after simulation for $^{28}Si + {}^{76}Ge$. Three energies were considered – one near the Coulomb barrier, second below the Coulomb barrier and third above the Coulomb barrier. From table 4.2, one can conclude that

at energy below the Coulomb barrier, evaporation residues are ^{102}Pd, ^{101}Pd, ^{101}Rh, ^{98}Ru. Also, % residual yield of ^{101}Pd is highest among all evaporation residues. From table 4.3 i.e. at energy near the Coulomb barrier, evaporation residues are ^{101}Pd, ^{100}Pd, ^{100}Rh, ^{97}Ru and % residual yield of ^{100}Pd is highest among all evaporation residuals. The E/V_b for ^{28}Si + ^{76}Ge will be 0.98021 for energy 85 MeV. Also, from table 4.4 i.e. at energy above the Coulomb barrier, the obtained number of evaporation residues with significant yield is more in number. These are ^{100}Pd, ^{100}Rh, ^{99}Pd, ^{99}Rh, ^{97}Ru, ^{96}Ru. From table 4.2 to 4.4, one can conclude that for below barrier ^{101}Pd is most populated, for near barrier ^{100}Pd is populated and for above barrier ^{99}Pd is most populated. This is because as the beam energy is increased, the compound nucleus is populated in higher excited state and hence, can evaporate larger number of particles. Another observation is that neutron evaporation channels are preferred because of the absence of the Coulomb barrier.

For ^{30}Si + ^{74}Ge:

(i) Below the Coulomb barrier

Table 4.5 Evaporation residues along with their Z, N, A, % yields, cross-section at energy below the Coulomb barrier for ^{30}Si + ^{74}Ge.

Z	N	A	Evaporation Residue	Events	%	x-section	Channel
46	52	102	Pd	6792	67.9%	1.24E-05	2n
46	55	101	Pd	738283	73.8%	5.81E-06	3n
45	56	101	Rh	139894	14%	9.43E-07	1p2n
44	54	98	Ru	73777	7.38%	6.69E-07	2p4n

(ii) Near the Coulomb barrier

Table 4.6 Evaporation residues along with their Z, N, A, % yields, cross-section at an energy near the Coulomb barrier.for $^{30}Si + ^{74}Ge$.

Z	N	A	Evaporation Residue	Events	%	x-section	Channel
46	55	101	Pd	81054	8.11%	25.1	3n
46	54	100	Pd	535518	53.6%	166	4n
45	55	100	Rh	195146	19.5%	60.4	1p3n
44	53	97	Ru	91138	9.11%	28.2	2p5n

(iii) Above Coulomb barrier

Table 4.7 Evaporation residues along with their Z, N, A, % yields, cross-section at an energy above the Coulomb barrier for 30Si + 74Ge. for $^{30}Si + ^{74}Ge$.

Z	N	A	Evaporation Residue	Events	%	x-section	Channel
46	54	100	Pd	139692	14%	114	4n
45	55	100	Rh	76015	7.6%	62.1	1p3n
46	53	99	Pd	248079	24.8%	203	5n
45	54	99	Rh	235099	23.5%	192	1p4n
44	53	97	Ru	75610	7.56%	61.8	2p5n
44	52	96	Ru	130911	13.1%	107	2p6n

From above tables, one can conclude following about evaporation residues which are obtained after simulation for $^{30}Si + ^{74}Ge$. Here also three energies were considered – one near the Coulomb barrier, second below the Coulomb barrier and third above the Coulomb barrier. From table 4.5, one can

conclude that at energy below the Coulomb barrier, evaporation residues are ^{102}Pd, ^{101}Pd, ^{101}Rh, ^{98}Ru. Also, % residual yield of ^{101}Pd is highest among all evaporation residual. From table 4.6 i.e. at energy near the Coulomb barrier, evaporation residues are ^{101}Pd, ^{100}Pd, ^{100}Rh, ^{97}Ru and % residual yield of ^{100}Pd is highest among all evaporation residuals. The E/V_b for ^{28}Si + ^{76}Ge will be 1.037 for energy 90 MeV. Also, from table 4.7 i.e. at energy above the Coulomb barrier, the obtained number of evaporation residues with significant yield is more in number. These are ^{100}Pd, ^{100}Rh, ^{99}Pd, ^{99}Rh, ^{97}Ru, ^{96}Ru. From table 4.2 to 4.7, one can conclude that all evaporation residues are similar for both the systems. From tables 4.5 to 4.7, it can be concluded that for below barrier ^{101}Pd is most populated, for near barrier ^{100}Pd is populated and for above barrier ^{99}Pd is most populated. This result is same as that for ^{28}Si + ^{76}Ge.

4.5 ANGULAR DISTRIBUTION OF EVAPORATION RESIDUES

Angular distribution of evaporation residues in reactions of ^{28}Si with ^{76}Ge at different energies for the Coulomb barrier is plotted from Fig 4.4 to 4.6.

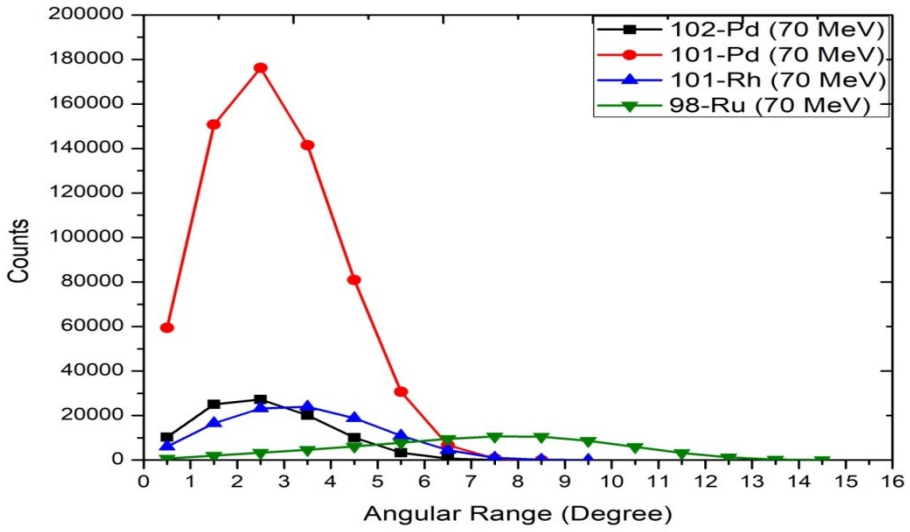

Fig 4.4 Angular distribution of different evaporation residues obtained below the Coulomb barrier for ^{28}Si + ^{76}Ge.

From Fig. 4.4, one can conclude that at beam energy of 70 MeV, ^{101}Pd has highest number of counts/yield when angular range is in between 2 to 3 degree. Also, ^{102}Pd is most forward focused as

compared to ^{101}Pd or ^{101}Rh and lastly one would observe ^{98}Ru has peak around 7-8 degree. It is clear from these simulations that as the number of evaporated particles increases, the recoiling nuclei will be peaked at higher values of angular range.

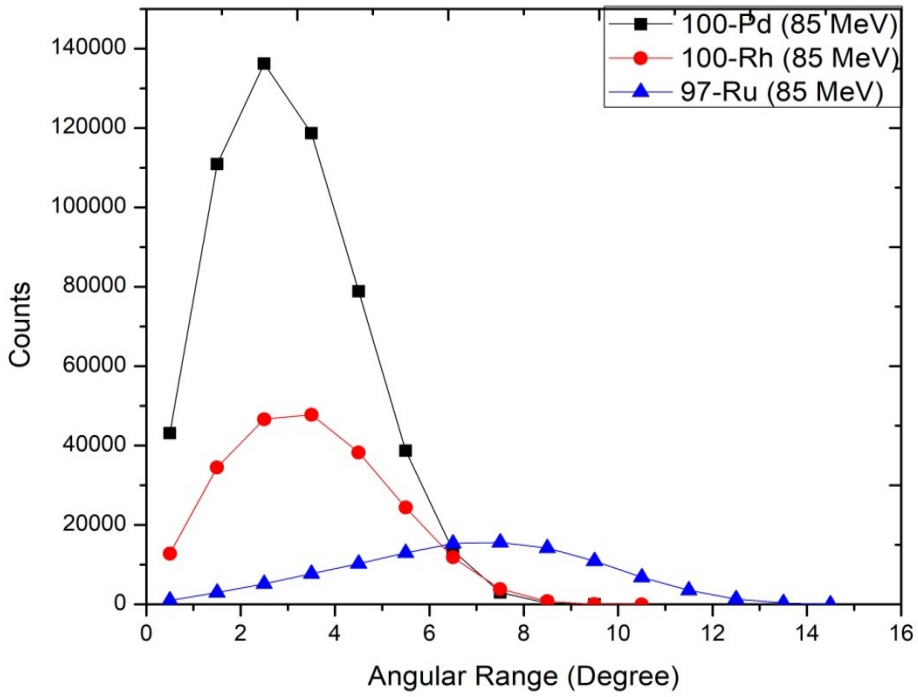

Fig. 4.5: Angular distribution of different evaporation residue obtained at an energy near the Coulomb barrier for ^{28}Si + ^{76}Ge.

From fig. 4.5, one may conclude that at beam energy of 85 MeV, ^{100}Pd will have higher number of counts/yields when angular range is in between 2 to 3 degree. Also, ^{100}Rh is observed to be forward focused as compared to others. Lastly, ^{97}Ru will have peak around 7-8 degree. Reason is as same as discussed for previous figures. From fig. 4.6, ^{99}Pd will have higher number of counts/yields when angular range is between 2 to 3 degrees. ^{96}Ru is observed to be forward focused as compared to others. Lastly, ^{97}Ru will have peak around 7-8 degree.

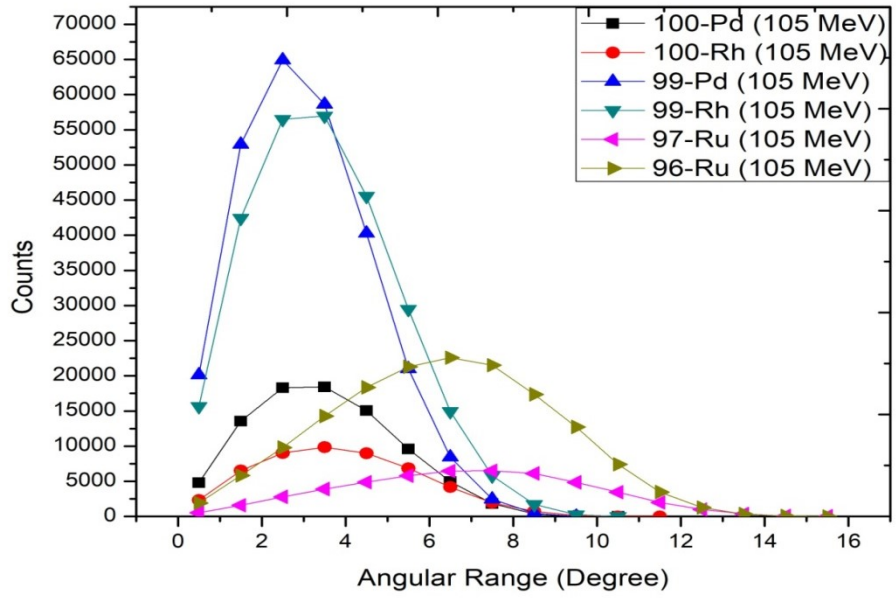

Fig. 4.6 Angular distribution of different evaporation residue obtained at an energy above the Coulomb barrier for $^{28}Si + ^{76}Ge$.

Angular distribution of evaporation residues in reactions of ^{30}Si with ^{74}Ge at different energies around the Coulomb barrier is plotted from Fig 4.7 to 4.9.

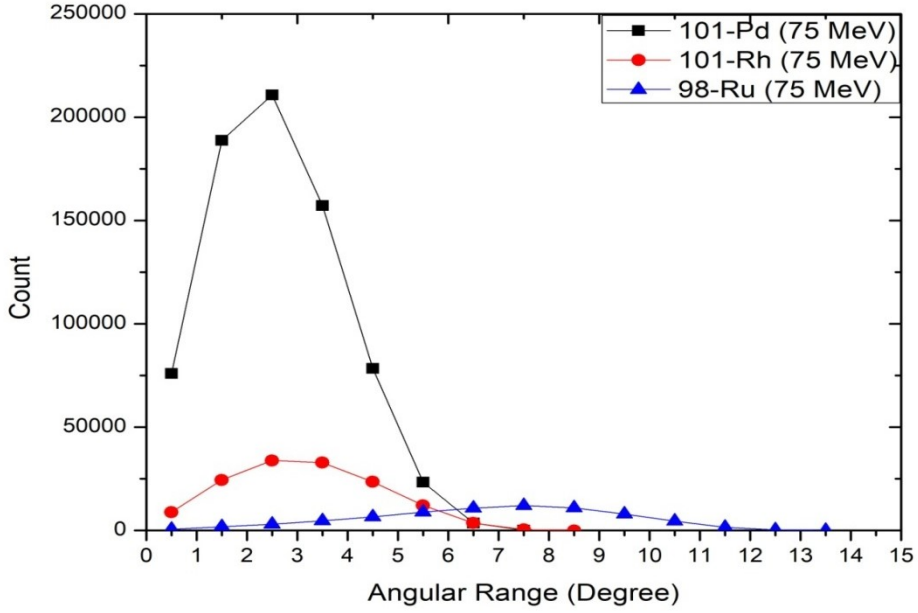

Fig. 4.7 Angular Range versus counts of different evaporation residue obtained below Coulomb barrier for $^{30}Si + ^{74}Ge$.

From Fig. 4.7, one can conclude that at beam energy of 75 MeV, ^{101}Pd has highest number of counts/yield when angular range is in between 2 to 3 degree. Also, ^{101}Rh is most forward focused as compared to ^{101}Pd and lastly one would observe ^{98}Ru has peak around 7-8 degree.

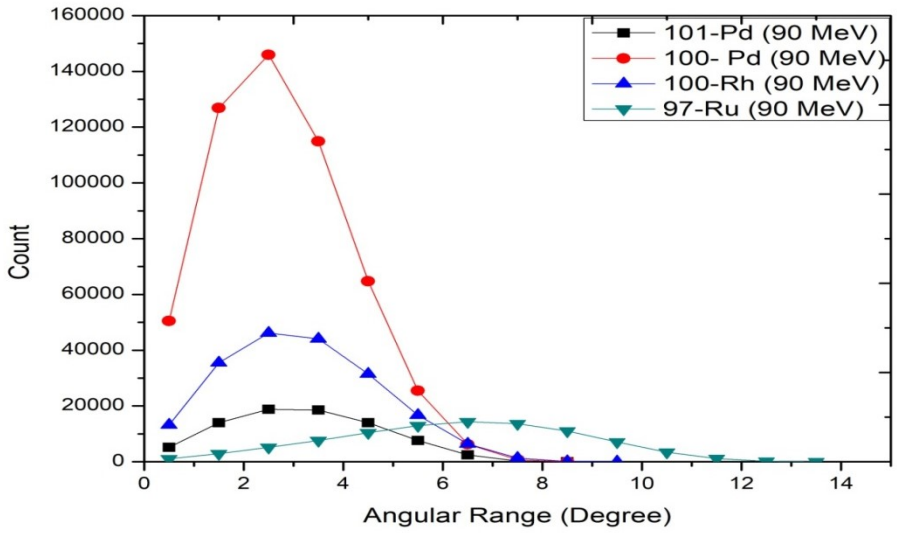

Fig. 4.8 Angular Range versus counts of different evaporation residue obtained near Coulomb barrier for ^{30}Si + ^{74}Ge.

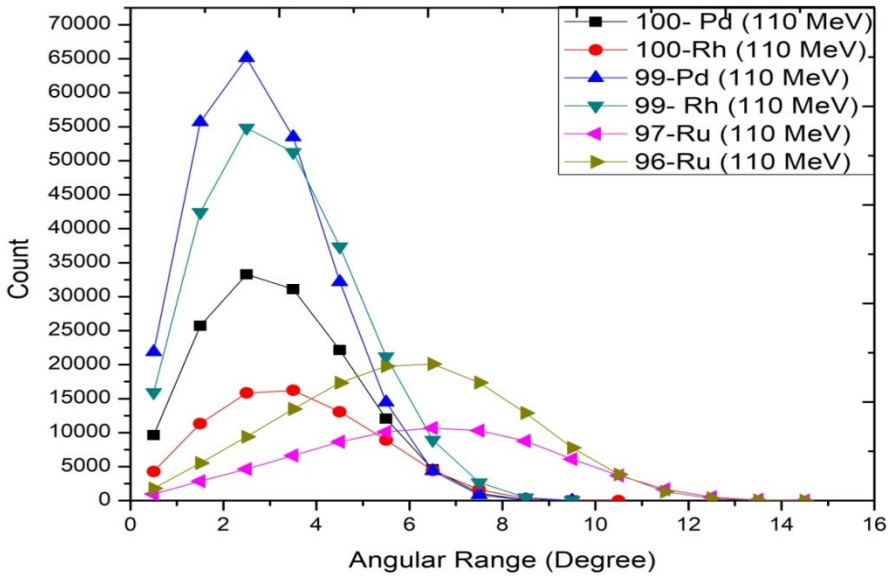

Fig. 4.9 Angular Range versus Counts of different Evaporation Residue obtained above Coulomb barrier for ^{30}Si + ^{74}Ge.

From Fig. 4.8, one can conclude that at beam energy of 90 MeV, ^{100}Pd has highest number of counts/yield when angular range is in between 2 to 3 degree. Also, ^{100}Rh is most forward focused as compared to ^{101}Pd and lastly one would observe ^{97}Ru has peak around 7-8 degree. From Fig. 4.9, one can conclude that at beam energy of 110 MeV, ^{99}Pd has highest number of counts/yield when angular range is in between 2 to 3 degree. Also, ^{100}Rh is most forward focused as compared to ^{101}Pd and lastly one would observe ^{97}Ru has peak around 7-8 degree.

4.6 ENERGY SPECTRA OF DIFFERENT EVAPORATION RESIDUES

Excitation energy of evaporation residues is plotted at different energies in Fig. 4.10 and 4.11 for reactions of ^{28}Si with ^{76}Ge and ^{30}Si with ^{74}Ge

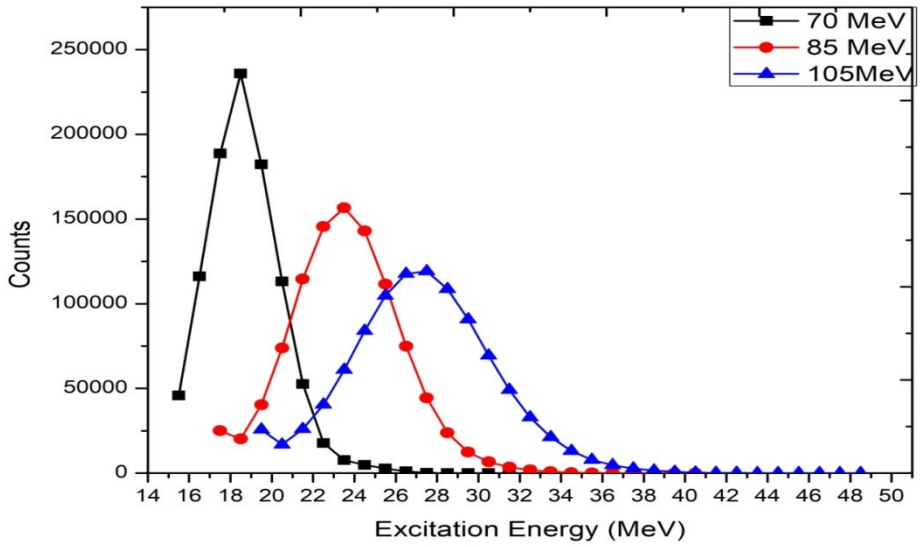

Fig. 4.10 Excitation energy distribution at different energies (below, near and above the Coulomb barrier) for ^{28}Si + ^{76}Ge.

In fig. 4.10 i.e. excitation energy distribution at different energies (below, near and above the Coulomb barrier) for ^{28}Si + ^{76}Ge is shown. As beam energy is increased, the peak of excitation energy also moves to higher excitation energy. This happens because as beam energy increases, it results into the increase in excitation energy. Fig. 4.11 shows Excitation energy distribution at different energies (below, near

and above the Coulomb barrier) for $^{30}Si + ^{74}Ge$. The obtained observations are same. One can conclude as beam energy is increased, the peak of excitation energy also increases. As excitation energy increases, counts will decrease and curve obtained is forward focus.

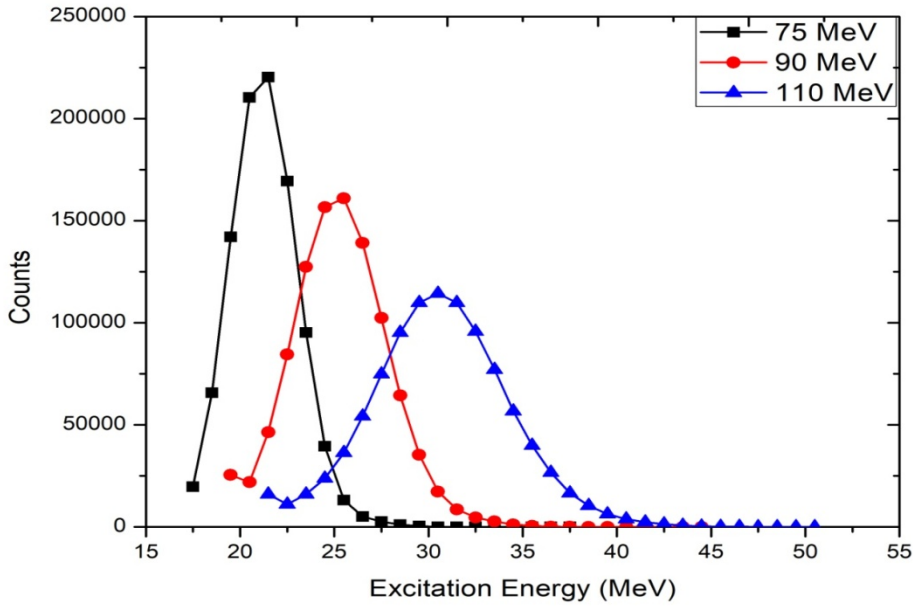

Fig. 4.11 Excitation energy distribution at different energies (below, near and above the Coulomb barrier) for $^{30}Si + ^{74}Ge$.

4.7 ANGULAR DISTRIBUTION FOR DIFFERENT PARTICLES

Fig. 4.12 to 4.14 shows angular distributions for neutron, proton and alpha particles at different energies for ^{28}Si with ^{76}Ge. This was done by taking log $_{10}$(counts) vs. angular range. From fig. 4.12, one may conclude that unlike other particles, neutrons do not experience Coulomb barrier, which will show large reaction cross sections for neutrons at a very low energy. Thus we observe angular distribution of neutron particles to be high among all other particles. One may conclude that for energy below the Coulomb barrier, at angular range 20˚ to 140˚ observed counts are almost same i.e. plateau like region is obtained. In fig. 4.13 and 4.14, same observation is obtained as that in case of fig. 4.12. Fig. 4.13 and

4.14 is for angular distribution for neutron, proton and alpha particles at energy near and above Coulomb barrier.

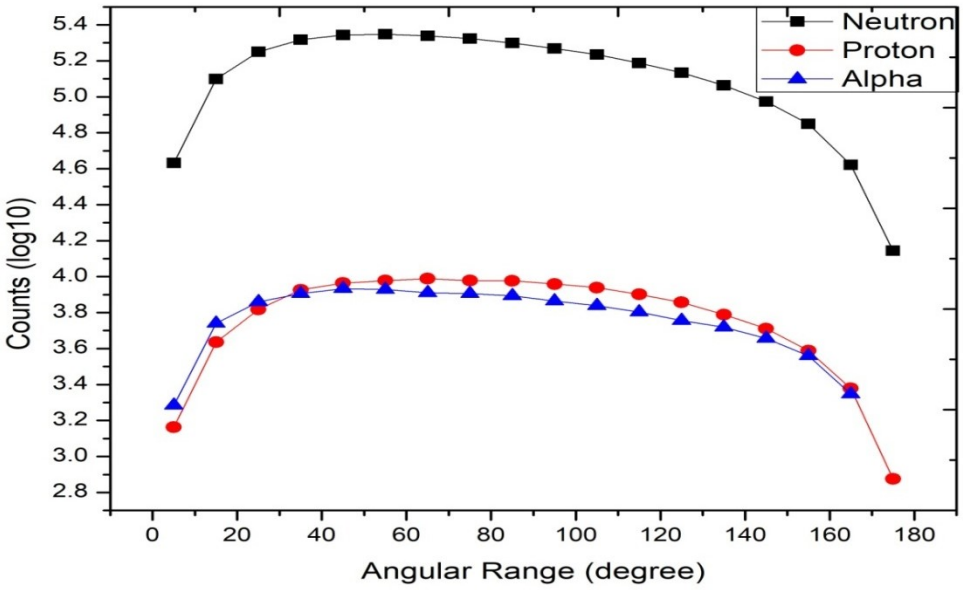

Fig. 4.12 Angular distribution for neutron, proton and alpha particles at energy below the Coulomb barrier for $^{28}Si + ^{76}Ge$.

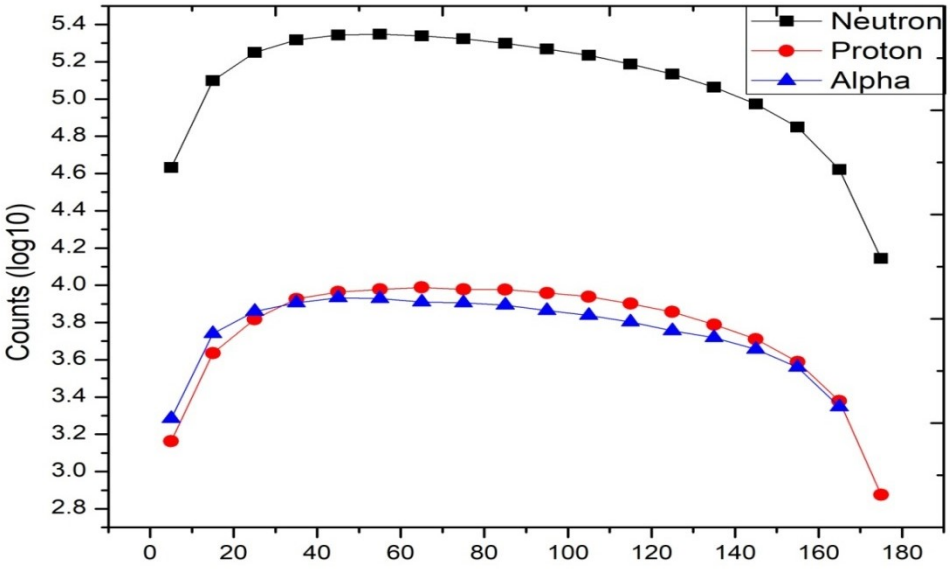

Fig. 4.13 Angular distribution for neutron, proton and alpha particles at an energy near the Coulomb barrier for $^{28}Si + ^{76}Ge$.

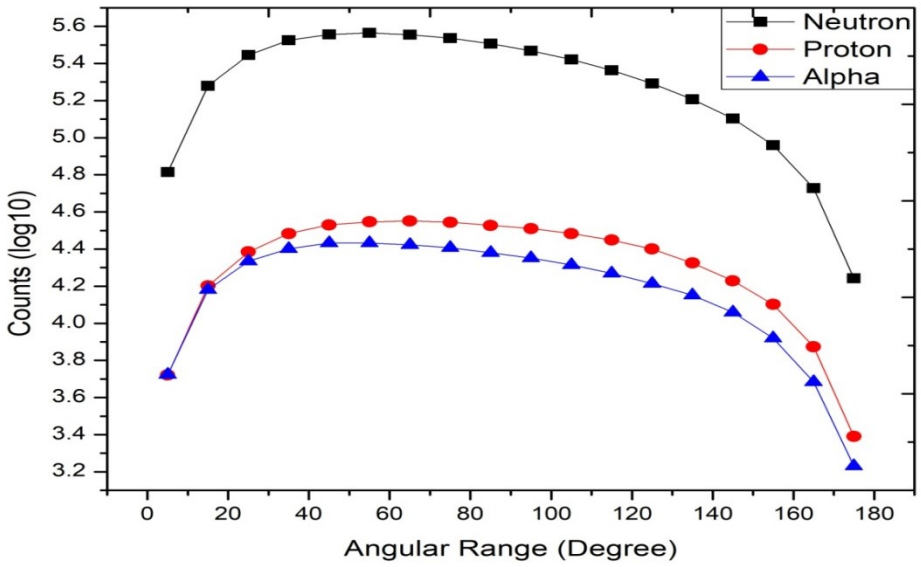

Fig. 4.14 Angular Range versus counts for neutron, proton versus alpha particles above Coulomb barrier for $^{28}Si + ^{76}Ge$.

Fig. 4.15 to 4.17 shows angular distributions for neutron, proton and alpha particle at different energies for ^{30}Si with ^{74}Ge.

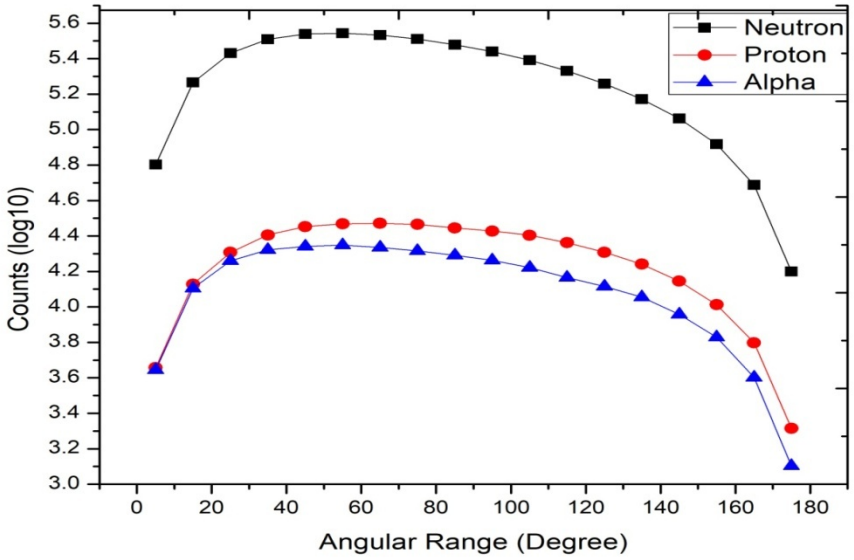

Fig. 4.15 Angular Range versus counts for neutron, proton and alpha particles below Coulomb barrier for $^{30}Si + ^{74}Ge$.

From fig. 4.15, one may conclude same observation like system $^{28}Si + ^{76}Ge$ that unlike other particles, neutrons do not experience Coulomb barrier, which will show large reaction cross sections for neutrons at a very low energy. Thus we observe angular distribution of neutron particles to be high among all other particles.

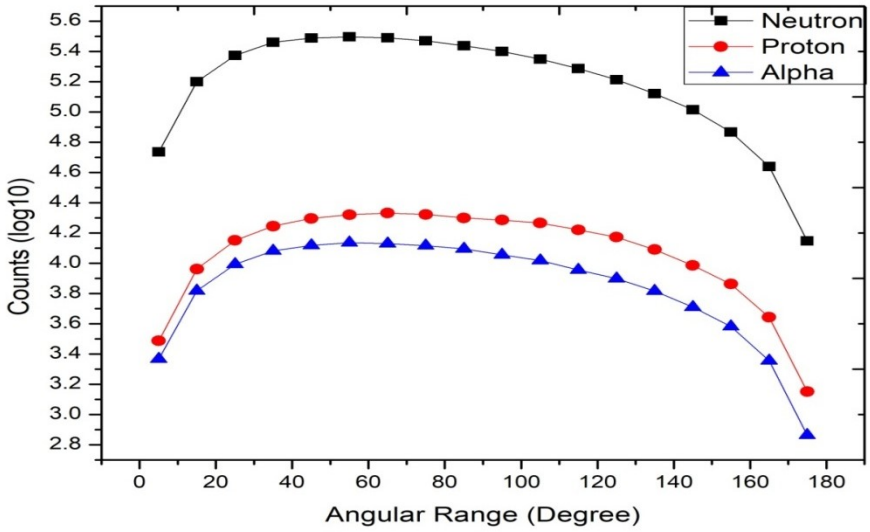

Fig. 4.16 Angular Range versus counts for neutron, proton and alpha particles near Coulomb barrier for $^{30}Si + ^{74}Ge$.

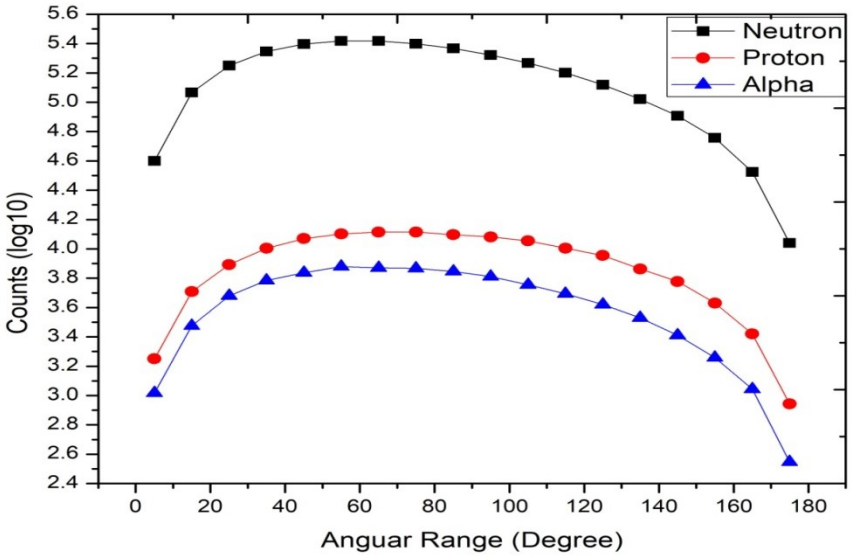

Fig. 4.17 Angular Range versus counts for neutron, proton and alpha particles above Coulomb barrier for $^{30}Si + ^{74}Ge$.

In fig. 4.16 and 4.17, same observation is obtained as that in case of fig. 4.12. Fig. 4.13 and 4.14 is for angular distribution for neutron, proton and alpha particles at energy near and above Coulomb barrier.

4.8 Summary and conclusions

In previous sections, various features of heavy ion fusion reactions around the Coulomb barrier are presented and discussed. So, conclusion of this thesis work is written below:

- System ^{28}Si with ^{76}Ge and ^{30}Si with ^{74}Ge is chosen so that, obtained compound nucleus ^{104}Pd is same after fusion. Simulations were carried out around the Coulomb barrier i.e. 20% below to 20% above the Coulomb barrier.
- If angular momentum, J versus partial cross-section, SIG (J) is plotted then as the beam energy is increased, partial cross section extends to higher values of angular momentum.
- Evaporation residues obtained at energy below the Coulomb barrier are ^{102}Pd, ^{101}Pd, ^{101}Rh, ^{98}Ru; at energy near the Coulomb barrier are ^{101}Pd, ^{100}Pd, ^{100}Rh, ^{97}Ru and at energy above the Coulomb barrier are ^{100}Pd, ^{100}Rh, ^{99}Pd, ^{99}Rh, ^{97}Ru, ^{96}Ru. Below barrier ^{101}Pd is most populated, for near barrier ^{100}Pd is populated and for above barrier ^{99}Pd is most populated. Some evaporation residues are populated at similar E/V_b for both systems.
- It was observed that less is number of evaporated nucleons, more forward focused is the recoiling evaporation residue.
- When excitation energy of evaporation residues is plotted at different energies then, as beam energy is increased, the peak of excitation energy moves to higher value.
- Angular distributions of various evaporated particles such as neutrons, protons and alpha particles are plotted. It was observed that distribution was flat and neutrons have the maximum yield.

REFERENCES

[1]European science foundation “Nuclear physics in the science of atomic nucleus and of nuclear matter.” (2010):6.

[2]Lamarsh.J.R, Barattta.A.J “Introduction to Nuclear Engineering (3rd Edition).”(1975).

[3]Krane.K.S “Introductory Nuclear Physics”, (1986) :416-431.

[4]M. Antonio “Models for nuclear reactions with weakly-bound systems.”(2019):5.

[5]Bertulani, Carlos A. "Nuclear reactions." *digital Encyclopedia of Applied Physics* (2009):14-16.

[6]Satou, K., et al. "Measurements of evaporation residue cross sections for the fusion reactions Kr^{86}+ Ba^{134} and Kr^{86}+ Ba^{138}." *Physical Review C* 73.3 (2006): 034609.

[7]Beckerman, M. "Sub-barrier fusion of two nuclei." *Reports on Progress in Physics* 51.8(1988):1047.

[8]Wong, C.Y. "Interaction barrier in charged-particle nuclear reactions." *Physical Review Letters* 31.12 (1973):766.

[9]Gavron, A. "Statistical model calculations in heavy ion reactions." *Physical Review C* 21.1(1980): 230.

[10]Tarasov O.B., D.Bazin. "Development of the program LISE: application to fusion–evaporation." *Nuclear Instruments and Methods in Physics Research Section B: Beam Interactions with Materials and Atoms* 204 (2003):174-178.

[11]Kalkal, Sunil, et al. "Channel coupling effects on the fusion excitation functions for Si^{28}+ $Zr^{90,94}$ in sub-and near-barrier regions." *Physical Review C* 81.4 (2010): 044610.

[12]Casten R.F. “ Nuclear structure from a simple perspective.”,(1990):360-364 .

[13]Jia, H. M., et al. "Fusion of the $^{16}O + ^{76}Ge$ and $^{18}O + ^{74}Ge$ systems and the role of positive Q-value neutron transfers." *Physical Review C* 86.4 (2012): 044621.

[14]Aljuwair, H. A., et al. "Isotopic effects in the fusion of Ca^{40} with $Ca^{40,44,48}$." *Physical Review C* 30.4 (1984):1223.

[15]Zhang, H. Q., et al. "Near-barrier fusion of $S^{32} + Zr^{90,96}$: The effect of multi-neutron transfers in sub-barrier fusion reactions." *Physical Review C* 82.5 (2010): 054609.

Submission ID: 1156052853

Garima Sharma MSc Thesis V01

ORIGINALITY REPORT

6%	1%	6%	1%
SIMILARITY INDEX	INTERNET SOURCES	PUBLICATIONS	STUDENT PAPERS

PRIMARY SOURCES

1	O.B. Tarasov, D. Bazin. "Development of the program LISE: application to fusion–evaporation", Nuclear Instruments and Methods in Physics Research Section B: Beam Interactions with Materials and Atoms, 2003 Publication	2%
2	Tapan Rajbongshi, Kushal Kalita. "Systematic study of deformation effects on fusion cross-sections using various proximity potentials", Open Physics, 2014 Publication	<1%
3	baadalsg.inflibnet.ac.in Internet Source	<1%
4	Canto, L.F.. "Fusion and breakup of weakly bound nuclei", Physics Reports, 200602 Publication	<1%
5	Manjeet Singh Gautam, Hitender Khatri, K. Vinod. "Role of nuclear structure degrees of freedom and energy dependent interaction potential in sub-barrier fusion dynamics",	<1%